Journal of Science and Technology – Smart Systems and Devices
Volume 36, Issue 2, May 2026, 001–010

An Enhanced Multi-Stream Spatial Modulation Scheme for High-Rate MIMO Systems

Minh-Tuan Le, Trung-Hieu Nguyen*

Posts and Telecommunications Institute of Technology, Ha Noi, Vietnam
**Corresponding author email: hieunt@ptit.edu.vn*

Abstract

This paper proposes an Enhanced Multi-Stream Spatial Modulation (En-MSM) system employing N_t transmit antennas, where two antennas are activated simultaneously, for high-rate MIMO systems. En-MSM conveys information bits through both the spatial domain, i.e., the indexes of the active antennas, and PAM/QAM symbols. Each transmit signal vector, or transmit codeword, includes one M-PAM and one conventional N-QAM symbol, with the M-PAM symbols generated as even multiples. To further improve spectral efficiency, the M-PAM symbols are combined to form new M-APSK symbols, which replace the PAM symbols in the transmit vector. This design expands the available transmit codeword set and increases the minimum distance in the signal space. A sub-optimal detector is also proposed for signal recovery in the En-MSM scheme to support scenarios requiring low detection complexity, at the expense of some performance degradation. Simulation results demonstrate that En-MSM achieves noticeable performance gains compared with conventional MSM, ESM, and GSM-MIM across various scenarios, while maintaining comparable hardware complexity. Moreover, compared with SM, En-MSM not only achieves significant performance gains but also requires substantially fewer transmit antennas.

Keywords: Generalized spatial modulation, index modulation, MIMO, multi-stream spatial modulation, spatial modulation.

1. Introduction

Space Modulation (SM) [1–4] is a multiple-input multiple-output (MIMO) technique introduced to address the main challenges of conventional MIMO systems–namely, high implementation complexity that increases with the number of antennas, antenna synchronization issues, and inter-symbol interference-by activating only a small number of transmit antennas at a time. Moreover, in many MIMO applications, hardware cost and energy consumption limit both mobile and fixed devices from being equipped with a large number of radio-frequency (RF) chains [5]. When the number of simultaneously active antennas, i.e., the number of RF chains, at the transmitter is smaller than the number of available transmit (TX) antennas, the resulting antenna redundancy can be exploited by mapping information onto the indices of the active antennas. In addition to conventional Quadrature-Amplitude-Modulation/Phase-Shift-Keying (QAM/PSK)-modulated symbols, SM leverages the spatial domain, namely, the position of the TX antennas, referred to as the Spatial Constellation (SC), to transmit extra bits [3]. The SC generated by an SM scheme depends on the chosen combination of active antennas, enabling information to be carried jointly by the signal and spatial constellations, thereby improving spectral efficiency.

Initially, SM was proposed with a single active antenna [1, 3]. This approach, however, could not achieve high spectral efficiency. Subsequent works generalized SM and SSK techniques by allowing multiple active antennas to transmit simultaneously, thereby relaxing the single RF-chain constraint. In [4], the authors introduced an extension of SM, known as generalized SM (GSM), in which more than one antenna is active during transmission. Specifically, during each symbol period, N_a out of N_t antennas are activated simultaneously to transmit symbols. As a result, the spectral efficiency of GSM is no longer limited to $\log_2(N_t)$ bits per channel use (bpcu), thus reducing the need for a very large number of transmit antennas. Nevertheless, to achieve high spectral efficiency for high-rate data transmission, a substantial number of antennas is still required.

In a recent work, Cheng *et al.* proposed Enhanced SM (ESM), a technique employing one or two active antennas and multiple constellations [5]. Its principles are: (1) symbols from a primary constellation are sent with one active antenna, while symbols from a secondary constellation are used with two; (2) secondary constellations, each half the size of the primary, ensure a consistent bit rate across both cases; and (3) these constellations are geometrically interpolated to maximize minimum Euclidean distance. ESM was shown to significantly improve spectral efficiency compared to SM and SMX while reducing ML detection complexity.

Cheng *et al.* later introduced three ESM designs for multistream SM (MSM), termed ESM-Type 1, 2, and 3 [6]. The designs preserved the primary constellation's

p-ISSN 3093-3285
e-ISSN 3093-3315
https://doi.org/10.51316/jst.190.ssad.2026.36.2.1
Received: Nov 11, 2025; Revised: Jan 21, 2026;
Accepted: Feb 11, 2026; Online: Mar 10, 2026.

minimum distance while lowering average transmit energy, yielding higher SNR gains at equal spectral efficiency. For 10-bpcu at CER 10^{-3}, the schemes achieved gains of about 0.6 dB, 1.3 dB, and 1.8 dB over MSM. This signal design approach has since been extended to improve efficiency and reliability across diverse MIMO applications [7, 8].

Following the introduction of QSM in [9], which improves the spectral efficiency of SM by expanding the number of spatial symbol combinations while retaining its main advantages, several generalized QSM (GQSM) schemes have been developed to further enhance efficiency by allowing multiple antennas to be active simultaneously [10–12]. In the GQSM scheme of [10], the transmit antenna array of size N_t is partitioned into $n_B = \frac{N_t}{2}$ groups. Each group processes one N-QAM symbol and, according to the QSM principle, activates either one or two antennas. Consequently, the resulting spectral efficiency of GQSM is $n_B(\log_2 N + 2)$ bpcu.

In [13], the Generalized Spatial Modulation with Multi-Index Modulation (GSM-MIM) scheme is proposed, extending the index dimension through two distinct constellations. By exploiting both spatial and index domains, GSM-MIM transmits more bits than conventional GSM. A Transmitted Spatial Vector (TSV) is formed by combining two spatial vectors: one mapped from an M-PAM symbol and the other from an L-QAM symbol. To further improve reliability, a modified M-PAM (MoPAM) constellation is introduced to enlarge the squared minimum Euclidean distance (SMED) between TSVs.

In this paper, we present a new design for Multi-Stream Spatial Modulation (MSM) systems employing N_t transmit antennas, where two antennas are active at each signaling interval. The proposed technique, referred to as Enhanced MSM (En-MSM), conveys information bits not only through spatial-constellation (SC) codewords but also via Pulse-Amplitude Modulation (PAM) and Quadrature-Amplitude Modulation (QAM) symbols transmitted from different antennas. It is noteworthy that our proposed scheme is fundamentally different from the ESM scheme in [5]. Specifically, ESM employs signal vectors that activate either one or two transmit antennas, whereas our proposed approach is a purely MSM-based scheme with exactly two active transmit antennas at any time.

The distinctive feature of En-MSM is that each transmit signal vector carries both an M-PAM and a conventional N-QAM symbol, with the PAM symbols restricted to even-valued amplitudes. To further improve spectral efficiency, the scheme enlarges the transmit codeword set by combining signal points from two PAM constellations to form a new Amplitude-and-Phase Shift Keying (APSK) constellation with M points (M-APSK), whose symbols replace the original M-PAM symbols in the transmit vector.

As a result, the scheme can generate a total of $\Lambda = (2+M)(N_t-1)N_t$ antenna combinations, from which $r = \lfloor \log_2 \Lambda \rfloor$ information bits can be transmitted, where $\lfloor \cdot \rfloor$ denotes the floor function. Consequently, the proposed scheme achieves a spectral efficiency of:

$$\zeta = [\log_2(NM) + r] \text{ bpcu} \tag{1}$$

To support application scenarios in which low detection complexity is required, a sub-optimal detector based on the existing OB-MMSE scheme [14] is proposed for signal recovery in the En-MSM scheme, at the cost of some performance degradation. The proposed detector, referred to as the modified OB-MMSE (M-OB-MMSE), differs from the original OB-MMSE in the following two aspects:

1) The OB-MMSE was developed to handle the case where the transmitted symbols are drawn from the same conventional QAM constellation. In contrast, the M-OB-MMSE must cope with symbols drawn from different modulation types, namely PAM, APSK, and QAM.

2) In the OB-MMSE, symbols are detected and Euclidean distances are evaluated until either the early stopping condition is met or all transmit antenna combinations (TACs) are tested, after which the final solution corresponding to the minimum Euclidean distance is selected. In contrast, in the M-OB-MMSE, symbols are recovered and the minimum distance is evaluated at each iteration. Once the minimum distance satisfies the early stopping condition, the detector terminates and outputs the final solution.

Simulation results demonstrate that the proposed scheme achieves substantial SNR gains compared with conventional SM, GSM-MIM, and ESM techniques at the same spectral efficiencies. In addition, the M-OB-MMSE provides significant complexity reduction compared with the ML detector, at the expense of some performance loss. Moreover, as the number of receive antennas increases, the resulting performance degradation becomes smaller.

The remainder of this paper is organized as follows. Section 2 presents the system model. Section 3 describes the proposed M-APSK constellations, transmit signal vectors, and achievable spectral efficiencies. S ection 4 evaluates the minimum Euclidean distance among the codewords of the proposed scheme. The development of the M-OB-MMSE detection algorithm is presented in Section 5. Section 6 presents the simulation results, and Section 7 concludes the paper.

2. System Model

Consider an MSM system operating over a MIMO channel with N_t transmit antennas and N_r receive antennas. The input bit vector $\mathbf{b}$ of length $(m+n+r)$

is mapped by the MSM transmitter into a transmit codeword:

$$\mathbf{c} = \begin{bmatrix} c_1 & c_2 & \cdots & c_{N_t} \end{bmatrix}^T \tag{2}$$

whose average energy is assumed to be:

$$E_c = \mathscr{E}\{\text{trace}(\mathbf{c}\mathbf{c}^H)\} \tag{3}$$

where $\mathscr{E}\{\cdot\}$ denotes the expectation, $(\cdot)^T$ and $(\cdot)^H$ denote the transpose and the Hermitian transpose of a matrix or vector, respectively. The codeword $\mathbf{c}$ is then transmitted over the MIMO channel by activating N_a out of N_t transmit antennas at each signaling interval.

At the receiver, the received signal vector can be expressed as:

$$\mathbf{y} = \mathbf{H}\mathbf{c} + \mathbf{n} \tag{4}$$

where $\mathbf{H}$ is the $N_r \times N_t$ channel matrix and $\mathbf{n}$ is the $N_r \times 1$ noise vector. The entries of $\mathbf{H}$ and $\mathbf{n}$ are modeled as independent and identically distributed (i.i.d.) complex Gaussian random variables with zero mean, with variances equal to 1 and σ^2, respectively.

The MSM receiver detects the transmitted codeword using a maximum-likelihood (ML) detector, given by:

$$\begin{aligned} \hat{\mathbf{c}} &= \arg\min_{\mathbf{c}} \|\mathbf{y} - \mathbf{H}\mathbf{c}\|^2 \\ &= \arg\min_{\mathbf{c}\in\mathscr{C}} \|\mathbf{y} - \mathbf{H}\mathbf{c}\|^2 \end{aligned} \tag{5}$$

where $\|\cdot\|$ denotes the Frobenius norm and $\mathscr{C}$ is the codebook of all possible MSM codewords.

According to [15], the MSM transmitter generate N_a N-QAM modulated symbols, each of which carries $\log_2 N$ bits, whereby resulting in a spectral efficiency of $\eta_{\text{MSM}} = \log_2(\Lambda) + N_a \log_2(N)$ bpcu, where $\Lambda = \binom{n_T}{2}$. For an MSM system with $N_t = 4$ and $N_a = 2$ employing N-QAM modulation, the transmitted codeword $\mathbf{c}$ is selected from the following signal space $\mathscr{C}$:

$$\mathscr{C} = \left\{ \begin{bmatrix} v_1 \\ v_2 \\ 0 \\ 0 \end{bmatrix} \quad \begin{bmatrix} v_1 \\ 0 \\ v_2 \\ 0 \end{bmatrix} \quad \begin{bmatrix} v_1 \\ 0 \\ 0 \\ v_2 \end{bmatrix} \quad \begin{bmatrix} 0 \\ v_1 \\ v_2 \\ 0 \end{bmatrix} \right\} \tag{6}$$

i.e., $\mathbf{c} \in \mathscr{C}$, where v_1 and v_2 are N-QAM symbols, i.e., $v_1, v_2 \in \Omega_N$.

3. Proposed Transmit PAM/QAM Constellation and Signal Vector Design

3.1. Proposed APSK Constellations

In [13], the authors proposed the M-MoPAM constellation given by:

$$\Omega_M = \{ \; -2m \quad \cdots \quad -2 \quad 2 \quad \cdots \quad 2m \; \}, \; m = \frac{M}{2} \tag{7}$$

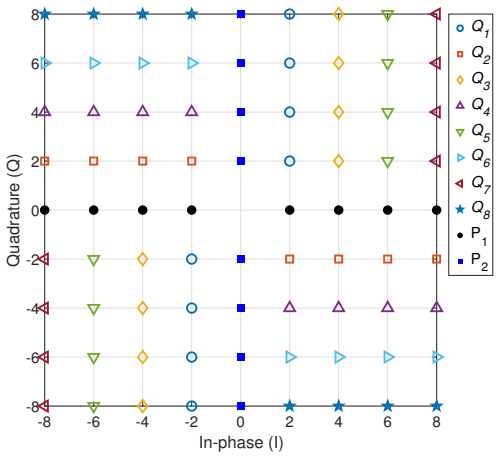

Fig. 1. Illustration of the M-PAM constellations and the proposed M-APSK constellations for $M = 8$

It can be seen from (7) that the elements of Ω_M are multiple of two. This is to guarantee maximum Euclidean distance among the transmit signal vectors of the GSM-MIM scheme.

Based on Ω_M, we construct two constellations, each of which has M signal points as follows:

$$\mathscr{P}_1 = \{-2m, \ldots, -2, 2, \ldots, 2m\} \tag{8a}$$
$$\mathscr{P}_2 = j\mathscr{P}_1 \tag{8b}$$

After that, using the signal points in $\mathscr{P}_1$ and $\mathscr{P}_2$, we then construct M APSK constellations, each of which has M signal points, as follows:

$$\begin{aligned} \mathscr{Q}_1 &= \{-2-2jm, \ldots, -2-2j, \\ &\qquad 2+2j, \ldots, 2+2jm\}, && \text{(9a)} \\ \mathscr{Q}_2 &= j\mathscr{Q}_1, && \text{(9b)} \\ \mathscr{Q}_3 &= \{-4-2jm, \ldots, -4-2j, \\ &\qquad 4+2j, \ldots, 4+2jm\}, && \text{(9c)} \\ \mathscr{Q}_4 &= j\mathscr{Q}_3, && \text{(9d)} \\ &\vdots \\ \mathscr{Q}_{M-1} &= \{-2m-2jm, \ldots, -2m-2j, \\ &\qquad 2m+2j, \ldots, 2m+2jm\}, && \text{(9e)} \\ \mathscr{Q}_M &= j\mathscr{Q}_{M-1}, && \text{(9f)} \end{aligned}$$

where j is the imaginary unit, i.e., $j^2 = -1$.

Illustrated in Fig. 1 are the diagrams of the 8-PAM and proposed 8-APSK constellations. It is observed that the signal points in the proposed constellations, $\mathscr{Q}_k$ for $k = 1, 3, \ldots, M-1$, lie in the first and third quadrants, whereas those in $\mathscr{Q}_k$ for $k = 2, 4, \ldots, M$, lie in the second and fourth quadrants. Meanwhile, the 8-PAM constellations $\mathscr{P}_1$ and $\mathscr{P}_2$ lie along the in-phase (I) and quadrature (Q) axes, respectively.

It can be easily verified that the average symbol energy of $\mathscr{P}_1$ and $\mathscr{P}_2$ equals:

$$E_{\mathscr{P}} = \frac{(M+1)(M+2)}{3}$$

and that the M-APSK constellations have average symbol energies as follows:

$$\begin{aligned} E_{\mathscr{Q},1} &= E_{\mathscr{Q},2} = \tfrac{1}{3}(M^2+3M+14) \\ E_{\mathscr{Q},3} &= E_{\mathscr{Q},4} = \tfrac{1}{3}(M^2+3M+50) \\ E_{\mathscr{Q},5} &= E_{\mathscr{Q},6} = \tfrac{1}{3}(M^2+3M+110) \\ &\cdots \\ E_{\mathscr{Q},M-1} &= E_{\mathscr{Q},M} = \tfrac{1}{3}(4M^2+3M+2) \end{aligned} \tag{10}$$

The average symbol energies of the M-APSK constellations increase with M. Hence, when combined with the spatial domain, redundant signal vectors containing higher-order APSK symbols are eliminated to ensure good bit error rate (BER) performance, as discussed below.

3.2. Proposed Transmit Signal Vectors

3.2.1. Two transmit antennas

With $N_t = 2$ transmit antennas, using the M-PAM in (8)-(8b), M-APSK in (9)-(9f) and the conventional N-QAM constellations, the transmitted signal vector, $\mathbf{c}$, in our proposed En-MSM technique can be drawn from the following signal space:

$$\mathscr{C} = \left\{ \begin{array}{l} \begin{bmatrix} x_1 \\ v \end{bmatrix}, \begin{bmatrix} v \\ x_1 \end{bmatrix}, \begin{bmatrix} x_2 \\ v \end{bmatrix}, \begin{bmatrix} v \\ x_2 \end{bmatrix}, \\ \begin{bmatrix} s_1 \\ v \end{bmatrix}, \begin{bmatrix} v \\ s_1 \end{bmatrix}, \begin{bmatrix} s_2 \\ v \end{bmatrix}, \begin{bmatrix} v \\ s_2 \end{bmatrix} \\ \vdots \\ \begin{bmatrix} s_{M-1} \\ v \end{bmatrix}, \begin{bmatrix} v \\ s_{M-1} \end{bmatrix}, \begin{bmatrix} s_M \\ v \end{bmatrix}, \begin{bmatrix} v \\ s_M \end{bmatrix} \end{array} \right\} \tag{11}$$

where $x_q \in \mathscr{P}_q$ for $q = 1,2$, $s_k \in \mathscr{Q}_k$ for $k = 1,2,\ldots,M$, and $v \in \Omega_N$.

As can be seen from (11), the total number of signal combinations is $4+2M$. Therefore, $\lfloor \log_2(4+2M) \rfloor$ information bits can be conveyed through the spatial domain. Compared with conventional SM and ESM schemes for the same number of transmit antennas, the number of combinations in the proposed scheme increases by factors of $\frac{2^{\lfloor \log_2(4+2M) \rfloor}}{2}$ and $\frac{2^{\lfloor \log_2(4+2M) \rfloor}}{8}$, respectively.

This demonstrates that the proposed scheme exploits the spatial domain much more efficiently than conventional SM and ESM. Using the $(4+2M)$ combinations in (11), the spectral efficiency of the proposed scheme can be expressed as:

$$\zeta = \lfloor \log_2(4+2M) \rfloor + \log_2(MN) \text{ bpcu}$$

3.2.2. Four transmit antennas

In the case of $N_t = 4$, the construction of the transmit signal vectors is straightforward due to the signal space defined in (11). For example, by using the first vector $\begin{bmatrix} x_1 \\ v \end{bmatrix}$ in (11), we can construct six transmit signal vectors as follows:

$$\left\{ \begin{bmatrix} x_1 \\ v \\ 0 \\ 0 \end{bmatrix}, \begin{bmatrix} x_1 \\ 0 \\ v \\ 0 \end{bmatrix}, \begin{bmatrix} x_1 \\ 0 \\ 0 \\ v \end{bmatrix}, \begin{bmatrix} 0 \\ x_1 \\ v \\ 0 \end{bmatrix}, \begin{bmatrix} 0 \\ x_1 \\ 0 \\ v \end{bmatrix}, \begin{bmatrix} 0 \\ 0 \\ x_1 \\ v \end{bmatrix} \right\} \tag{12}$$

Since there are 16 combinations in (11), these can be extended to form a transmit signal space $\mathscr{C}$ consisting of 64 antenna combinations for $N_t = 4$. Consequently, the spectral efficiency of the proposed scheme is given by $6 + \log_2(2N)$ bpcu.

With $(4+2M)$ combinations in (11), we can extend to $6(4+2M)$ antenna combinations for $N_t = 4$. The spectral efficiency of the proposed scheme can be evaluated as:

$$\zeta = \lfloor \log_2(24+12M) \rfloor + \log_2(MN) \text{ bpcu} \tag{13}$$

3.2.3. N_t transmit antennas

In general, for a given N_t, using the first vector $\begin{bmatrix} x_1 \\ v \end{bmatrix}$ in (11), we are able to construct $\binom{N_t}{2}$ signal combinations as follows:

$$\mathbf{c} \in \left\{ \begin{bmatrix} x_1 \\ v \\ 0 \\ \vdots \\ 0 \end{bmatrix}, \begin{bmatrix} x_1 \\ 0 \\ v \\ \vdots \\ 0 \end{bmatrix}, \ldots, \begin{bmatrix} 0 \\ \vdots \\ 0 \\ x_1 \\ v \end{bmatrix}, \begin{bmatrix} 0 \\ \vdots \\ 0 \\ v \\ x_1 \end{bmatrix} \right\} \tag{14}$$

Consequently, with $(4+2M)$ combinations in (11), we can extend to Λ antenna combinations as follows:

$$\Lambda = \binom{N_t}{2}(4+2M) = (2+M)(N_t-1)N_t. \tag{15}$$

The spectral efficiency of the proposed scheme can be evaluated as:

$$\zeta = \lfloor \log_2(\Lambda) \rfloor + \log_2(MN) \text{ bpcu} \tag{16}$$

Since $\gamma = 2^{\lfloor \log_2(\Lambda) \rfloor} < \Lambda$, the number of redundant signal vectors is equal to $(\Lambda - \gamma)$. In the proposed scheme, these unused signal vectors correspond to those with the largest averaged symbol energies, which are determined based on the average symbol energies given in (10).

Table 1 presents a comparison of the spectral efficiencies of different SM schemes with $N_t = 4$ and 8, considering the cases where $N_a = 1$, $N_a = 2$, or both. The results clearly show that the proposed En-MSM scheme achieves the largest number of antenna combinations for

Table 1. Spectral efficiencies of the proposed scheme compared with existing SM schemes for $N_t = 4$ and $N_t = 8$.

Schemes	**Spectral Efficiency** ζ (bpcu)	
	$N_t = 4$	$N_t = 8$
Proposed	$\lfloor \log_2(24+12M) \rfloor + \log_2(MN)$	$\lfloor \log_2(112+56M) \rfloor + \log_2(MN)$
SM [1]	$2+\log_2 N$	$3+\log_2 N$
GSM [4]	$2+\log_2 N$	$4+\log_2 N$
MSM [15]	$2+2\log_2 N$	$4+2\log_2 N$
ESM [5]	$4+\log_2 N$	$6+\log_2 N$

a given N_t. Consequently, it provides noticeable gains in spectral efficiency compared with SM, GSM, and ESM. For instance, when $M = 4$, $N = 64$, and $N_t = 8$, the proposed En-MSM scheme achieves a spectral efficiency of 16 bpcu, which is equal to that of MSM and is 7 bpcu higher than SM, 6 bpcu higher than GSM, and 4 bpcu higher than ESM.

3.3. Bit Mapping in the Proposed En-MSM Scheme

For a given input bit vector $\mathbf{b}$ of length $(m+n+r)$, the En-MSM transmitter first calculates the total number of transmit signal vectors, i.e., the cardinality of $\mathscr{C}$, given by $|\mathscr{C}| = 2^r$. Next, it computes the number of Transmit Antenna Combinations (TACs) as:

$$\Gamma = 2\binom{N_t}{2} = N_t(N_t-1) \tag{17}$$

and determines the number of M-PAM and M-APSK constellations to be employed as:

$$\Pi = \left\lceil \frac{|\mathscr{C}|}{\Gamma} \right\rceil \tag{18}$$

where $\lceil \cdot \rceil$ denotes the ceiling operator. Since there are always two M-PAM constellations and at most M M-APSK constellations, the maximum value of Π is $M+2$. For convenience, both the M-PAM and M-APSK constellations are hereafter referred to as M-APSK constellations.

As described in Subsection 3.2, for each M-APSK constellation, all Γ TACs are adopted. Therefore, if $\Pi \times \Gamma > |\mathscr{C}|$ a number of TACs must be eliminated. In this case, the number of TACs used with the last M-APSK constellation, i.e., the Π-th constellation, is given by:

$$\Xi = |\mathscr{C}| - (\Pi-1)\Gamma \tag{19}$$

Finally, the information bits are mapped into the transmit signal vectors as follows:

1) The last r bits are mapped to a transmit signal vector selected from the given transmit signal space $\mathscr{C}$. This step also determines which of the proposed M-APSK constellations, either $\mathscr{P}_q$ for $q = 1,2$ or $\mathscr{Q}_k$ for $k = 1,2,\ldots,\Pi-2$, is used for the subsequent bit mapping.
2) The first m bits are mapped to one of the signal points in the selected M-APSK constellation determined in Step 1).
3) The middle n bits are mapped to one of the signal points in the conventional N-QAM constellation.

After the above mapping steps, a transmit signal vector $\mathbf{c}$ is generated and transmitted to the receiver.

4. Evaluation of Minimum Euclidean Distance

In this section, we evaluate the minimum Euclidean distance among the transmit signal vectors of the proposed scheme. According to the rank and determinant criteria presented in [16], the squared Euclidean distance between two transmit signal vectors, $\mathbf{c}_i$ and $\mathbf{c}_j$, where $i \neq j$, in the proposed scheme is given by:

$$\delta_{ij} = \|\mathbf{c}_i - \mathbf{c}_j\|^2 \tag{20}$$

Without loss of generality, we consider the case $N_t = 2$. The evaluation for $N_t > 2$ is similar and straightforward. From (11), we examine the following cases.

4.1. Case 1

When $\mathbf{c}_i = \begin{bmatrix} x_q & v \end{bmatrix}^T, \mathbf{c}_j = \begin{bmatrix} \hat{x}_q & \hat{v} \end{bmatrix}^T$, where $x_q, \hat{x}_q \in \mathscr{P}_q$, for $q = 1,2$, and $v, \hat{v} \in \mathscr{Q}_N$, we can write:

$$\begin{aligned} \delta_{ij}^1 = \left\|\mathbf{c}_i - \mathbf{c}_j\right\|^2 &= \left\| \begin{bmatrix} x_q \\ v \end{bmatrix} - \begin{bmatrix} \hat{x}_q \\ \hat{v} \end{bmatrix} \right\|^2 \\ &= |x_q - \hat{x}_q|^2 + |v - \hat{v}|^2 \end{aligned} \tag{21}$$

If $x_q = \hat{x}_q$, δ_{ij}^1 has the smallest value when v and $\hat{v}$ are neighbouring signal points. Without loss of generality, assuming that $v = 1 + j$ and $\hat{v} = 1 - j$, then $|v - \hat{v}|^2 = |2j|^2$. Therefore, we have:

$$\delta_{ij}^1 = |v - \hat{v}|^2 \geq |2j|^2 = 2^2 = 4 \tag{22}$$

If $v = \hat{v}$, δ_{ij}^1 has the smallest value when x_q and $\hat{x}_q$ are neighbouring signal points. Without loss of generality, assuming that $x_q = 2, \hat{x}_q = 4$ for $q = 1$ or $x_q = 2j, \hat{x}_q = 4j$ for $q = 2$, then $|x_1 - \hat{x}_1|^2 = |2|^2$ and $|x_2 - \hat{x}_2|^2 = |2j|^2$. Therefore, we have:

$$\delta_{ij}^1 = |x_q - \hat{x}_q|^2 \geq |2|^2 = |2j|^2 = 2^2 = 4 \tag{23}$$

From (22) and (23), it follows that $\delta_{ij,\min}^1 = 4$.

4.2. Case 2

When $\mathbf{c}_i = \begin{bmatrix} s_k & v \end{bmatrix}^T, \mathbf{c}_j = \begin{bmatrix} \hat{s}_k & \hat{v} \end{bmatrix}^T$, where $s_k, \hat{s}_k \in \mathscr{Q}_k$, for $k = 1,2,\cdots,M$, and $v, \hat{v} \in \mathscr{Q}_N$, we can write:

$$\begin{aligned} \delta_{ij}^2 = \left\|\mathbf{c}_i - \mathbf{c}_j\right\|^2 &= \left\| \begin{bmatrix} s_k \\ v \end{bmatrix} - \begin{bmatrix} \hat{s}_k \\ \hat{v} \end{bmatrix} \right\|^2 \\ &= |s_k - \hat{s}_k|^2 + |v - \hat{v}|^2 \end{aligned} \tag{24}$$

If $s_k = \hat{s}_k$, it is straightforward to have:

$$\delta_{ij}^2 = |v-\hat{v}|^2 \geq |2|^2 = |2j|^2 = 2^2 = 4 \tag{25}$$

If $v = \hat{v}$, δ_{ij}^2 has the smallest value when s_k and $\hat{s}_k$ are neighbouring signal points. Without loss of generality, assuming that $s_k = 2m+2j, \hat{s}_k = 2m+4j$ for $k = M-1$, then $|s_k - \hat{s}_k|^2 = |-2j|^2$. Therefore, we have:

$$\delta_{ij}^2 = |s_k - \hat{s}_k|^2 \geq |-2j|^2 = 2^2 = 4 \tag{26}$$

From (25) and (26), it follows that $\delta_{ij,\min}^2 = 4$.

4.3. Case 3

When $\mathbf{c}_i = \begin{bmatrix} x_q & v \end{bmatrix}^T, \mathbf{c}_j = \begin{bmatrix} s_k & v \end{bmatrix}^T$, where $x_q \in \mathscr{P}_q$, for $q = 1,2$, $s_k \in \mathscr{Q}_k$, $k = 1,2,\cdots,M$, and $v, \hat{v} \in \mathscr{Q}_N$, we can write:

$$\begin{aligned}\delta_{ij}^3 = \left\|\mathbf{c}_i - \mathbf{c}_j\right\|^2 &= \left\| \begin{bmatrix} x_q \\ v \end{bmatrix} - \begin{bmatrix} s_k \\ v \end{bmatrix} \right\|^2 \\ &= |x_q - s_k|^2 \end{aligned} \tag{27}$$

for $q = 1,2$; and $k = 1,2,\cdots,M$.

δ_{ij}^3 in (27) attains its minimum value when x_q and s_k are closest. Without loss of generality, assuming that $x_1 = -2, s_1 = -2-2j$ for $q = k = 1$ or $x_2 = -2j, s_1 = -2-2j$ for $q = 2, k = 1$, then $|x_1 - s_1|^2 = |2j|^2$ and $|x_2 - s_1|^2 = |2|^2$. Therefore, we have:

$$\delta_{ij}^3 = |x_q - s_k|^2 \geq 2^2 = 4 \tag{28}$$

It follows from (28) that $\delta_{ij,\min}^3 = 4$.

4.4. Case 4

When $\mathbf{c}_i = \begin{bmatrix} x_q & v \end{bmatrix}^T, \mathbf{c}_j = \begin{bmatrix} v & x_q \end{bmatrix}^T$, where $x_q \in \mathscr{P}_q$, for $q = 1,2$, and $v \in \mathscr{Q}_N$, we can write:

$$\begin{aligned}\delta_{ij}^4 = \left\|\mathbf{c}_i - \mathbf{c}_j\right\|^2 &= \left\| \begin{bmatrix} x_q \\ v \end{bmatrix} - \begin{bmatrix} v \\ x_q \end{bmatrix} \right\|^2 \\ &= |x_q - v|^2 + |v - x_q|^2 = 2|x_q - v|^2, \quad q = 1,2 \end{aligned} \tag{29}$$

δ_{ij}^4 in (29) attains its minimum value when x_q and v are closest. Without loss of generality, assume that $x_1 = -2$, or $x_2 = -2j$ and $v = -1-j$. Then, $|x_1 - v|^2 = |-1+j|^2$ and $|x_2 - v|^2 = |1-j|^2$. Therefore, for the M-PAM and conventional N-QAM constellations, we always have: $|x_q - v|^2 \geq |-1+j|^2 = |1-j|^2 = |1+j|^2 = |-1-j|^2 = 2$, and hence:

$$\delta_{ij}^4 = 2|x_q - v|^2 \geq 2 \times 2 = 4. \tag{30}$$

It follows from (30) that $\delta_{ij,\min}^4 = 4$.

Similarly, by evaluating the remaining cases such as:

$$\mathbf{c}_i = \begin{bmatrix} s_k & v \end{bmatrix}^T, \quad \mathbf{c}_j = \begin{bmatrix} v & s_k \end{bmatrix}^T, \tag{31}$$

where $s_k \in \mathscr{Q}_k$ for $k = 1,2,\cdots,M$ and $v \in \mathscr{Q}_N$, or

$$\mathbf{c}_i = \begin{bmatrix} x_q & v \end{bmatrix}^T, \quad \mathbf{c}_j = \begin{bmatrix} v & s_k \end{bmatrix}^T, \tag{32}$$

where $x_q \in \mathscr{P}_q$, for $q = 1,2$, $s_k \in \mathscr{Q}_k$, $k = 1,2,\cdots,M$, and $v \in \mathscr{Q}_N$, we can obtain the minimum squared Euclidean distance of the proposed scheme as follows:

$$\delta_{\min} = \max_{\forall(\mathbf{c}_i,\mathbf{c}_j),n} \delta_{ij,\min}^n = 4. \tag{33}$$

The normalized minimum squared Euclidean distance of the proposed En-MSM scheme is given by:

$$\bar{\delta}_{\min} = \frac{\delta_{\min}}{\bar{E}_s} = \frac{4}{\bar{E}_s}, \tag{34}$$

where $\bar{E}_s = \frac{1}{2^\zeta}\sum_{i=1}^{2^\zeta} \mathbf{c}_i^H \mathbf{c}_i$ is the average codeword energy.

Using an exhaustive computer search, we obtained the minimum squared Euclidean distances for different spectral efficiencies with $N_t = 4$ and $N_a = 2$, as shown in Table 2. As observed, for the same spectral efficiency ζ, the proposed En-MSM achieves the smallest $\delta_{\min}$. For example, at $\zeta = 14$ bpcu, the $\delta_{\min}$ of En-MSM is $\frac{4}{57.5}$, whereas those of ESM, GSM-MIM, and MSM are $\frac{4}{204.5}$, $\frac{4}{112}$, and $\frac{4}{84}$, respectively. Consequently, the proposed En-MSM is expected to outperform all the compared schemes.

Table 2. Comparison of normalized minimum squared Euclidean distance for $N_t = 4$ and $N_a = 2$

ζ (bpcu)	$\bar{\delta}_{\min}$			
	Proposed En-MSM	**ESM** [5]	**GSM-MIM** [13]	**MSM** [15]
10	$\frac{4}{15}$	$\frac{4}{28.5}$	$\frac{4}{20}$	$\frac{4}{20}$
11	$\frac{4}{21.5}$	$\frac{4}{51.25}$	$\frac{4}{30}$	$\frac{4}{30}$
12	$\frac{4}{25.5}$	$\frac{4}{75.5}$	$\frac{4}{50}$	$\frac{4}{40}$
13	$\frac{4}{35.5}$	$\frac{4}{108}$	$\frac{4}{72}$	$\frac{4}{62}$
14	$\frac{4}{57.5}$	$\frac{4}{204.5}$	$\frac{4}{112}$	$\frac{4}{84}$

5. Sub-Optimal Signal Detection

5.1. Modified OB-MMSE Detector

This section presents a sub-optimal detector based on the OB-MMSE one presented in [14]. First, the ML detector in (5) is re-expressed as [14]:

$$\left(\hat{\Upsilon}, \hat{\mathbf{x}}\right) = \arg \min_{\Upsilon \in \Omega_\Upsilon, \mathbf{x} \in \Omega_x} \|\mathbf{y} - \mathbf{H}_\Upsilon \mathbf{x}\|^2 \tag{35}$$

where $\Omega_\Upsilon = \{\Upsilon_1, \Upsilon_2, \cdots, \Upsilon_\Gamma\}$, Υ_i, for $i = 1,2,\cdots,\Gamma$, is the i-th TAC, and Ω_x denotes the set of all 2×1 modulation symbol vectors.

Similar to the OB-MMSE detector, an ordering algorithm is first applied to the received signal vector of the proposed En-MSM scheme to sort the possible TACs. More specifically, the pseudo-inverse of each channel column is computed to preprocess the received vector

$\mathbf{y}$ so as to obtain:

$$\mathbf{u} = [u_1, u_2, \ldots, u_{N_t}]^T \tag{36}$$

where $u_l = (\mathbf{h}_l)^{\dagger}\mathbf{y}$, $(\mathbf{h}_l)^{\dagger} = \frac{\mathbf{h}_l^H}{\mathbf{h}_l^H \mathbf{h}_l}$, and $l \in \{1, 2, \ldots, N_t\}$.

To measure the reliability of each TAC, a weighting factor w_i is adopted as:

$$w_i = |u_{i1}|^2 + |u_{i2}|^2, \tag{37}$$

where $i \in \{1, 2, \ldots, \Gamma\}$. After that, the weighting factors are sorted to obtain the ordered TACs as

$$[l_1, l_2, \ldots, l_\Gamma] = \arg \operatorname{sort}(\mathbf{w}) \tag{38}$$

where $\mathbf{w} = [w_1, w_2, \ldots, w_\Gamma]^T$ is the weighting vector and $\operatorname{sort}(\cdot)$ denotes an ordering function that rearranges the elements of the input vector in descending order. Here, l_1 and l_Γ represent the indices corresponding to the maximum and minimum values of $\mathbf{w}$, respectively.

For each possible TAC that has been ordered, a simplified block MMSE detector with dimension $N_R \times 2$ is employed to detect the symbol vector $\hat{\mathbf{x}}_{j,q} = \begin{bmatrix} \hat{x}_q & \hat{v} \end{bmatrix}_j^T$ or the symbol vector $\hat{\mathbf{x}}_{j,k} = \begin{bmatrix} \hat{s}_k & \hat{v} \end{bmatrix}_j^T$ from the j-th TAC, which is given by:

$$\hat{\mathbf{x}}_{j,q} = \arg \min_{\hat{s}_q \in \mathscr{P}_q, v \in \Omega_N} \|\tilde{\mathbf{y}}_{l_j} - \mathbf{x}_{j,q}\|_F^2, \tag{39}$$

$$\hat{\mathbf{x}}_{j,k} = \arg \min_{\hat{s}_k \in \mathscr{Q}_k, v \in \Omega_N} \|\tilde{\mathbf{y}}_{l_j} - \mathbf{x}_{j,k}\|_F^2 \tag{40}$$

where $\tilde{\mathbf{y}}_{l_j} = \left((\mathbf{H}_{\Upsilon_{l_j}})^H \mathbf{H}_{\Upsilon_{l_j}} + \sigma^2 \mathbf{I}\right)^{-1} (\mathbf{H}_{\Upsilon_{l_j}})^H \mathbf{y}$ denotes the MMSE-equalized received signal vector, $\mathbf{I}$ is the 2×2 identity matrix, and Υ_{l_j} denote the l_j-th TAC.

Because the elements $\tilde{\mathbf{y}}_{l_j,1}$ and $\tilde{\mathbf{y}}_{l_j,1}$ of $\tilde{\mathbf{y}}_{l_j}$ are just the functions of s_q, s_k, or v without any interferences, equations (39) and (40) can be equivalently expressed as follows:

$$\hat{v} = \arg \min_{v \in \Omega_N} |\tilde{\mathbf{y}}_{l_j,2} - v|^2 \tag{41}$$

$$\hat{x}_q = \arg \min_{\hat{x}_q \in \mathscr{P}_q} |\tilde{\mathbf{y}}_{l_j,1} - x_q|^2, q = 1, 2 \tag{42}$$

$$\hat{s}_k = \arg \min_{\hat{s}_k \in \mathscr{Q}_k} |\tilde{\mathbf{y}}_{l_j,1} - s_k|^2, k = 1, 2, \cdots, M \tag{43}$$

From this point onward, minor modifications are applied to the OB-MMSE algorithm. Specifically, the modified OB-MMSE algorithm initially sets $d_{\min} = \infty$. It then detects v using (41). Next, for each q, it detects x_q using (42), evaluates $d_q = \left\|\mathbf{y} - \mathbf{H}_{\Upsilon_{l_j}} \hat{\mathbf{x}}_{j,q}\right\|_F^2$, and compares d_q with $d_{\min}$. If $d_q < d_{\min}$, the algorithm updates $d_{\min} = d_q$ and stores the optimal TAC $\hat{\Upsilon} = \Upsilon_{k_j}$ together with the corresponding recovered symbol vector $\hat{\mathbf{x}} = \hat{\mathbf{x}}_{j,q}$.

Similarly, for each k, it detects s_k using (43), evaluates $d_k = \left\|\mathbf{y} - \mathbf{H}_{\Upsilon_{l_j}} \hat{\mathbf{x}}_{j,k}\right\|_F^2$, and compares d_k with $d_{\min}$. If $d_k < d_{\min}$, the algorithm updates $d_{\min} = d_k$ and stores the optimal TAC $\hat{\Upsilon} = \Upsilon_{k_j}$ along with the corresponding recovered symbol vector $\hat{\mathbf{x}} = \hat{\mathbf{x}}_{j,k}$.

To reduce the computational complexity required to detect all Γ possible TACs, the modified OB-MMSE detector terminates and output the final solutions $\left(\hat{\Upsilon}, \hat{\mathbf{x}}\right)$ if the minimum distance d_{min} satisfies:

$$d_{min} \leq V_{\text{th}} \tag{44}$$

where $V_{\text{th}} = 2N_r\sigma^2$ is a predefined threshold for evaluating the reliability of the detected signal vector [14]. Otherwise, the detector updates $j = j + 1$ and continues with the next estimate ($j \leq \Gamma$).

The modified OB-MMSE (M-OB-MMSE) detection algorithm is summarized in Algorithm 1.

5.2. Complexity Evaluation

In this subsection, we evaluate the computational complexity of the ML and M-OB-MMSE detectors under the assumption that one real addition, subtraction, multiplication, or division is counted as one floating-point operation (flop). A complex addition requires two flops, while a complex multiplication requires six flops. The multiplication or division of a complex number by a real number is counted as two flops, and a complex division is counted as eleven flops. Due to space limitations, only the final results are presented.

The total computational complexity of the ML detector, expressed in terms of flops per bit, is given by:

$$C_{\text{ML}}^{\text{b}} = \frac{2^\zeta (23N_r - 1)}{\zeta} \quad \text{flops/bit} \tag{45}$$

Similarly, the worst-case computational complexity of the M-OB-MMSE detector without the early stopping condition, expressed in terms of flops per bit, is given by:

$$C_{\text{M-OB,max}}^{\text{b}} = \frac{N_t(15N_r - 1) + (48N_r + 83 + 9N)\Gamma}{\zeta} + \frac{(9M + 23N_r - 2)\Pi\Gamma}{\zeta} \quad \text{flops/bit} \tag{46}$$

6. Simulation Results

In this section, we evaluate the bit error rate (BER) performance of the proposed En-MSM scheme and compare it with several existing SM-based schemes, namely SM [1], GSM [4], MSM [15], ESM [5], and the GSM-MIM method in [13]. The analysis assumes that the transmitted signals propagate over a quasi-static Rayleigh fading channel, and all schemes employ brute-force maximum-likelihood (ML) detector as in (5) for signal recovery.

Algorithm 1. Modified OB-MMSE Detection Algorithm for En-MSM Scheme

Input: $\mathbf{y}, \mathbf{H}, N_t, 2, \mathbf{I}, V_{\text{th}} = 2N_r\sigma^2, d_{min} = \infty$

1) Compute $u_l = (\mathbf{h}_l)^{\dagger}\mathbf{y}, \quad (\mathbf{h}_l)^{\dagger} = \frac{\mathbf{h}_l^H}{\mathbf{h}_l^H\mathbf{h}_l}$, and form $\mathbf{u} = [u_1, u_2, \ldots, u_{N_t}]^T$.
2) Compute $w_i = \sum_{k=1}^{2} |u_{ik}|^2, \quad i \in \{1, 2, \ldots, \Gamma\}$, and form $\mathbf{w} = [w_1, w_2, \ldots, w_\Gamma]^T$.
3) Sort $\mathbf{w}$ in ascending order:

$[l_1, l_2, \ldots, l_\Gamma] = \arg\text{sort}(\mathbf{w})$.

4) Initialize $j = 1$.
5) **While** $j \leq \Gamma$:

a) Compute

$$\tilde{\mathbf{y}}_{l_j} = \left((\mathbf{H}_{\Upsilon_{l_j}})^H \mathbf{H}_{\Upsilon_{l_j}} + \sigma^2\mathbf{I}\right)^{-1} (\mathbf{H}_{\Upsilon_{l_j}})^H \mathbf{y}.$$

b) Detect: $\hat{v} = \arg\min_{v \in \Omega_N} |\tilde{\mathbf{y}}_{l_j,2} - v|^2$.
c) **For** $q = 1:2$
Detect: $\hat{x}_q = \arg\min_{\hat{x}_q \in \mathscr{P}_q} |\tilde{\mathbf{y}}_{l_j,1} - x_q|^2$.
Compute $d_q = \left\|\mathbf{y} - \mathbf{H}_{\Upsilon_{l_j}} \hat{\mathbf{x}}_{j,q}\right\|_F^2$.
If $d_{min} > d_q$
$d_{min} = d_q$, $\hat{\Upsilon} = \Upsilon_{k_j}$, $\hat{\mathbf{x}} = \hat{\mathbf{x}}_{j,q}$.
Endif
Endfor
d) **For** $k = 1 : \Pi - 2$
Detect: $\hat{s}_k = \arg\min_{\hat{s}_k \in \mathscr{Q}_k} |\tilde{\mathbf{y}}_{l_j,1} - s_k|^2$.
Compute $d_k = \left\|\mathbf{y} - \mathbf{H}_{\Upsilon_{l_j}} \hat{\mathbf{x}}_{j,k}\right\|_F^2$.
If $d_{min} > d_k$
$d_{min} = d_k$, $\hat{\Upsilon} = \Upsilon_{k_j}$, $\hat{\mathbf{x}} = \hat{\mathbf{x}}_{j,k}$.
Endif
Endfor
e) **If** $d_{min} < V_{\text{th}}$: **break**.
Endif
f) $j = j + 1$.
Endwhile

Output: Detected $(\hat{\Upsilon}, \hat{\mathbf{x}})$ for bit de-mapping.

Fig. 2 presents the BER performance of the proposed En-MSM scheme compared with SM, conventional MSM, and ESM for $N_t = 4$ and $N_r = 4$, all achieving a spectral efficiency of 14 bpcu. Except for SM, which employs a single RF chain, the other schemes use two RF chains with appropriately selected constellations to maintain the target rate. As observed in Fig. 2, En-MSM outperforms conventional MSM in the high-SNR region and provides noticeable performance gains over SM, ESM, and GSM-MIM. At a BER of 10^{-3}, it achieves SNR improvements of approximately 6.1 dB, 2.5 dB, and 1.5 dB relative to SM, ESM, and GSM-MIM, respectively. Moreover, at a BER of 10^{-5}, En-MSM exhibits an additional improvement of nearly 0.75 dB in SNR compared with conventional MSM.

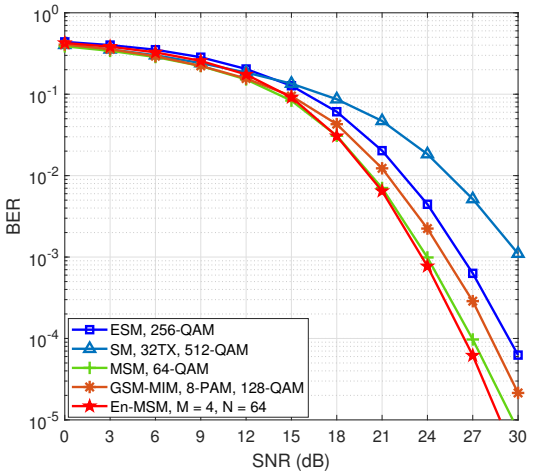

Fig. 2. Bit error rate performance of the proposed En-MSM, SM, GSM, conventional MSM, and ESM schemes for $N_t = 4$ and $N_r = 4$, all achieving a spectral efficiency of 14 bpcu

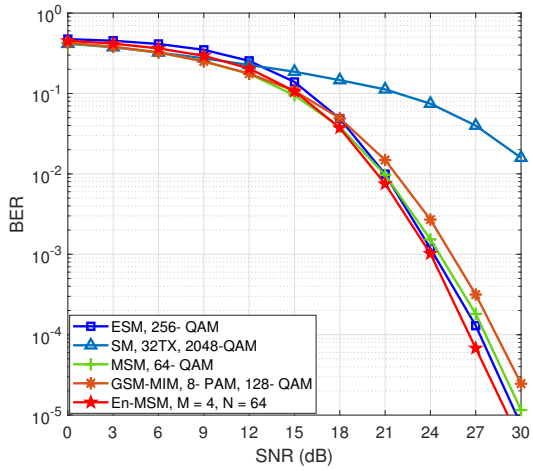

Fig. 3. Bit error rate performance of the proposed En-MSM, conventional MSM, ESM, and GSM-MIM schemes for $N_t = 8$ and $N_r = 4$, as well as SM with $N_t = 32$; all achieving a spectral efficiency of 16 bpcu

Fig. 3 presents the BER performance of the proposed En-MSM scheme compared with conventional MSM, ESM, and GSM-MIM (for $N_t = 8$, $N_r = 4$) and SM (for $N_t = 32$, $N_r = 4$). All schemes achieve a spectral efficiency of 16 bpcu. As observed in Fig. 3, the proposed En-MSM consistently outperforms the benchmark schemes. At a BER of 10^{-4}, En-MSM provides SNR gains of approximately 0.75 dB, 1 dB, and 1.75 dB over ESM, conventional MSM, and GSM-MIM, respectively. At a BER of 10^{-2}, it achieves an improvement of more than 9 dB compared with SM ($N_t = 32$). In addition, in terms of hardware complexity, En-MSM requires 24 fewer antennas than SM, indicating a more efficient design for high-rate communication systems.

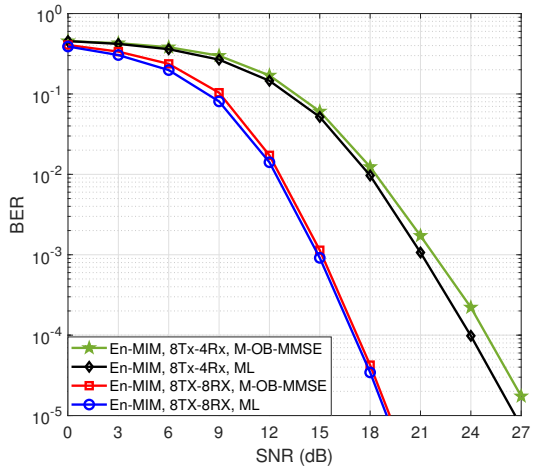

Fig. 4. Bit error rate performance of the proposed En-MSM scheme detected by the ML detector and the M-OB-MMSE detector for $N_t = 8$ with $N_r = 4$ and $N_r = 8$, at a spectral efficiency of 14 bpcu

Fig. 4 shows the BER performance of the proposed En-MSM scheme detected by the ML detector and the M-OB-MMSE detector for two antenna configurations, namely $(N_t = 8, N_r = 4)$ and $(N_t = 8, N_r = 8)$. Other parameters include $M = 4$, $N = 16$, and a spectral efficiency of $\zeta = 14$ bpcu. As can be observed from Fig. 4, when $N_r = 4$, the M-OB-MMSE detector underperforms the ML detector by approximately 1.2 dB at a BER of 10^{-4}. However, this performance gap is significantly reduced to about 0.3 dB as the number of receive antennas increases to $N_r = 8$.

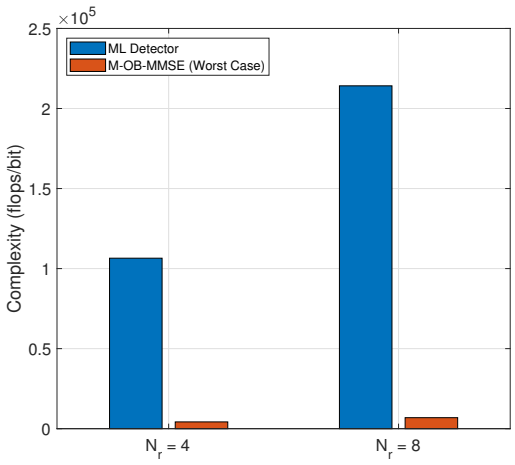

Fig. 5. Comparison of the complexity of the ML detector and the worst-case complexity of the M-OB-MMSE detector for $N_t = 8$ with $N_r = 4$ and $N_r = 8$, at a spectral efficiency of 14 bpcu

Fig. 5 compares the computational complexity of the ML detector and the worst-case complexity of the M-OB-MMSE detector for detecting the En-MSM scheme under the same system configurations as those used in Fig. 4. It is evident from Fig. 5 that the M-OB-MMSE detector offers significantly lower computational complexity compared to its ML counterpart. Specifically, when $N_r = 4$, the ML detector requires approximately 1.06×10^5 flops, whereas the M-OB-MMSE detector requires only 4226 flops. This means that the complexity of the M-OB-MMSE detector is roughly 4% of that of the ML detector, indicating a substantial reduction in detection complexity. As N_r increases to 8, the complexity reduction becomes even more pronounced, with 6872 flops required for the M-OB-MMSE detector compared to 2.1×10^5 flops for the ML detector.

The results presented in both Fig. 4 and Fig. 5 clearly highlight the main advantage of the M-OB-MMSE detector in terms of computational efficiency, albeit at the cost of some performance degradation. Therefore, when computational complexity is a primary concern, the M-OB-MMSE detector represents a promising candidate for signal recovery in the proposed En-MSM scheme.

7. Conclusion

In this paper, an Enhanced Multi-Stream Spatial Modulation (En-MSM) scheme is proposed for systems with N_t transmit antennas, where $N_a = 2$ antennas are simultaneously activated, to enhance the performance of conventional Multi-Stream Spatial Modulation (MSM). In En-MSM, each transmit vector consists of either one M-PAM symbol and one conventional N-QAM symbol, with the M-PAM symbols restricted to even multiples, or a newly designed M-APSK symbol that replaces the M-PAM symbol. Analytical results show that this approach enlarges the set of available transmit signal vectors and improves the minimum Euclidean distance among neighboring vectors in the signal space. Simulation results further confirm that En-MSM outperforms existing schemes, including GSM-MIM, ESM, conventional MSM, and SM, in terms of BER performance. For the same spectral efficiency, it not only provides significant performance gains over GSM-MIM and SM but also requires far fewer transmit antennas than SM, thereby reducing hardware complexity. Both simulation and analytical results also demonstrate that the M-OB-MMSE detector is capable of achieving near-ML performance with significantly lower complexity than the ML detector, particularly as the number of receive antennas increases. These advantages suggest that En-MSM is a promising candidate for future wireless MIMO systems employing spatial modulation.

References

[1] R. Mesleh, H. Haas, C. Ahn, and S. Yun, Spatial modulation – a new low complexity spectral efficiency enhancing technique, in Proc. First International Conference on Communications and Networking, Beijing, China, 2006, pp. 1–5.

[2] R. Mesleh, H. Haas, S. Sinanovic, C. W. Ahn, and S. Yun, Spatial modulation, IEEE Trans. Veh. Technol. vol. 57, no. 4, pp. 2228–2241, July 2008.
https://doi.org/10.1109/TVT.2007.912136

[3] M. Di Renzo, H. Haas, and P. M. Grant, Spatial modulation for multiple-antenna wireless systems: a survey, IEEE Commun. Mag. vol. 49, no. 12, pp. 182–191, Dec. 2011.
https://doi.org/10.1109/MCOM.2011.6094024

[4] A. Younis, N. Serafimovski, R. Mesleh, and H. Haas, Generalised spatial modulation, in Proc. Signals, Syst. Comput. Pacific Grove, CA, USA, 2010, pp. 1498–1502.

[5] C. Cheng, H. Sari, S. Sezginer, and Y. T. Su, Enhanced spatial modulation with multiple signal constellations, IEEE Trans. Commun. vol. 63, no. 6, pp. 2237–2248, June 2015.
https://doi.org/10.1109/TCOMM.2015.2422306

[6] C.-C. Cheng, H. Sari, S. Sezginer, and Y. T. Su, New signal designs for enhanced spatial modulation, IEEE Trans. Wireless Commun. vol. 15, no. 11, pp. 7766–7777, Nov. 2016.
https://doi.org/10.1109/TWC.2016.2607173

[7] M. Wei, S. Sezginer, G. Gui, and H. Sari, Bridging spatial modulation with spatial multiplexing: frequency-domain ESM, IEEE J. Sel. Top. Signal Process. vol. 13, no. 6, pp. 1326–1335, Oct. 2019.
https://doi.org/10.1109/JSTSP.2019.2913131

[8] F. Huang and Z. Zhou, Joint multiple constellations and variable active antennas selection for signal spaces design in MIMO systems, IEEE Trans. Commun. vol. 72, no. 2, pp. 1239–1251, Feb. 2024.
https://doi.org/10.1109/TCOMM.2023.3330861

[9] R. Mesleh, S. S. Ikki, and H. M. Aggoune, Quadrature spatial modulation, IEEE Trans. Veh. Technol. vol. 64, no. 6, pp. 2738–2742, June 2015.
https://doi.org/10.1109/TVT.2014.2344036

[10] F. R. Castillo-Soria, J. Cortez-Gonzalez, R. Ramirez-Gutierrez, F. M. Maciel-Barboza, and L. Soriano-Equigua, Generalized quadrature spatial modulation scheme using antenna grouping, ETRI J. vol. 39, no. 5, pp. 707–717, Oct. 2017.
https://doi.org/10.4218/etrij.17.0117.0162

[11] J. Li, S. Dang, Y. Yan, Y. Peng, S. Al-Rubaye, and A. Tsourdos, Generalized quadrature spatial modulation and its application to vehicular networks with NOMA, IEEE Trans. Intell. Transp. Syst. vol. 22, no. 7, pp. 4030–4039, July 2021.
https://doi.org/10.1109/TITS.2020.3006482

[12] J. An, C. Xu, Y. Liu, L. Gan, and L. Hanzo, The achievable rate analysis of generalized quadrature spatial modulation and a pair of low-complexity detectors, IEEE Trans. Veh. Technol. vol. 71, no. 5, pp. 5203–5215, May 2022.
https://doi.org/10.1109/TVT.2022.3155244

[13] Y. Zhan and F. Huang, Generalized spatial modulation with multi-index modulation, IEEE Commun. Lett. vol. 24, no. 3, pp. 585–588, Mar. 2020.
https://doi.org/10.1109/LCOMM.2019.2963183

[14] Y. Xiao, Z. Yang, L. Dan, P. Yang, L. Yin, and W. Xiang, Low-complexity signal detection for generalized spatial modulation, IEEE Communications Letters, vol. 18, no. 3, pp. 403–406, 2014.
https://doi.org/10.1109/LCOMM.2013.123113.132586

[15] K. Ntontin, M. Di Renzo, A. Perez-Neira, and C. Verikoukis, Performance analysis of multistream spatial modulation with maximum-likelihood detection, in Proc. IEEE Global Commun. Conf. (GLOBECOM), Atlanta, GA, USA, 2013, pp. 1590–1594.

[16] V. Tarokh, H. Jafarkhani, and A. R. Calderbank, Space-time block codes from orthogonal designs, IEEE Trans. Inf. Theory, vol. 45, no. 7, pp. 1456–1467, July 1999.
https://doi.org/10.1109/18.771146